Available online at www.sciencedirect.com

ScienceDirect

Solar Energy 126 (2016) 44–52

SOLAR ENERGY

www.elsevier.com/locate/solener

Tailoring optical absorption in silicon nanostructures from UV to visible light: A TDDFT study

Walid M.I. Hassan [a,b], M.P. Anantram [c], Reza Nekovei [d], Mahmoud M. Khader [a], Amit Verma [d,*]

[a] Gas Processing Center, College of Engineering, Qatar University, P.O. 2713, Qatar
[b] Chemistry Department, Faculty of Science, Cairo University, 12613 Giza, Egypt
[c] Department of Electrical Engineering, University of Washington, Seattle, WA 98195, USA
[d] Department of Electrical Engineering and Computer Science, Texas A&M University – Kingsville, Kingsville, TX 78363, USA

Received 22 June 2015; received in revised form 26 November 2015; accepted 30 November 2015
Available online 12 January 2016

Communicated by: Associate Editor Nicola Romeo

Abstract

The utilization of silicon nanostructures, from quantum dots to nanowires, for photovoltaic applications depends on understanding the effect of their physical structure on their optical absorption properties. In this work, we perform TDDFT calculations to study the length dependent optical absorption in pristine and doped silicon nanostructures. Our main findings are that: (i) The oscillator strength as a function of length is quadratic at small lengths, and then increases linearly. (ii) The exciton binding energy is seen to decrease by approximately 45% from 0.67 eV to about 0.3 eV with length increase, for a nanostructure with a cross-section diameter of approximately 12 Å. (iii) Doping and codoping with P, B, and Zr have the potential to cause the optical absorption to change from UV to the visible spectrum. The findings of this investigation demonstrate the potential to tailor silicon nanostructures for photovoltaic and optoelectronic applications.
© 2015 Elsevier Ltd. All rights reserved.

Keywords: Silicon nanostructures; Exciton binding energy; Doping; TDDFT

1. Introduction

Ultra-small silicon structures have gained significant attention for photovoltaic and other optoelectronic applications. Solar cells involving silicon quantum dots embedded in amorphous thin-films (the so-called third generation solar cells) have the potential to increase the efficiency of the solar cells (Conibeer et al., 2008). Silicon nanowires show considerable evidence from electrical transport measurements that active dopants can be incorporated during growth, (Xie et al., 2009; Cui et al., 2000, 2003; Wang and Dai, 2006; Zheng et al., 2004) and doping with either boron (B) or phosphorus (P) drastically changes the electrical transport character in silicon nanowires (Cui et al., 2000). P and B doped Si quantum dot based thin-films have shown lower electrical resistivity, which further promises higher efficiencies in solar cells (Hao et al., 2009a,b; Fukata et al., 2013). Si nanodots have demonstrated the potential to be critical components in nanoscale waveguide applications for photovoltaic and optoelectronics (Park et al., 2010). Silicon nanostructures (SNS) possess low reflectivity and stronger optical absorption (Adachi et al., 2010; Tsakalakos et al., 2007; Sivakov et al., 2009) in the

* Corresponding author.
E-mail address: Amit.Verma@tamuk.edu (A. Verma).

http://dx.doi.org/10.1016/j.solener.2015.11.030
0038-092X/© 2015 Elsevier Ltd. All rights reserved.

visible region compared to bulk and amorphous Si (Fukata et al., 2013; Adachi et al., 2010; Tsakalakos et al., 2007; Sivakov et al., 2009). SNS, by themselves, are also attractive candidates for such applications because of the tunability of the magnitude and nature of the band gap (direct or indirect) (Kocevski et al., 2013; Rand et al., 2007; Wong, 2009; Reining et al., 2002; Weissker et al., 2002).

Exciton binding energy is an important performance parameter that can govern the utilization of SNS in applications for solar cells. To a good approximation, the exciton binding energy can be defined as the difference between the transport or (fundamental) band gap and optical band gap (Rand et al., 2007; Wong, 2009; Reining et al., 2002; Garcia-Lastra and Thygesen, 2011). A material with a large exciton binding energy leads to the formation of an electron–hole pair that is tightly bound, which results in a poor material for solar cells because the electron–hole pair will eventually recombine rather than contribute to generating a current flow. The exciton binding energies are expected to decrease with the increase of the dimensions of the SNSs (Kupchak et al., 2006) but unfortunately the band gap shifts from direct to indirect with the transition in size (Kocevski et al., 2013). Surprisingly, the exciton binding energy of silicon nanocrystals (NCs) was found to decrease with increase in length (Parkash et al., 2011) and diameter (Kupchak et al., 2006) due to quantum confinement effects (Kocevski et al., 2013; Trani et al., 2005; Lu et al., 1995). Stable light emission of Si QDs and NCs is observed in the spectral range: blue (2.64–3.0 eV), green (2.25 eV), orange (2.05 eV), red (1.70–1.80 eV) and infrared (1.2–1.6 eV) (Shcherbyna and Torchynska, 2013; Cullis and Canham, 1991; Lehmann and Gosele, 1991; Prokes, 1993; Kanemitsu and Okamoto, 1997; Schuppler et al., 1995; Torchynska et al., 1999, 2005; Torchinskaya et al., 2003; Kim et al., 2003). These PL bands were attributed to exciton recombination in Si QDs, (Shcherbyna and Torchynska, 2013; Cullis and Canham, 1991; Lehmann and Gosele, 1991; Kanemitsu and Okamoto, 1997; Schuppler et al., 1995; Torchynska et al., 2005, 2006; Dybiec et al., 2004) the carrier recombination through defects inside of Si NCs (Torchynska et al., 2006), or via oxide related defects at the Si/SiOx interface (Shcherbyna and Torchynska, 2013; Prokes, 1993; Torchynska et al., 1999, 2005; Dybiec et al., 2004).

As SNS are being considered and incorporated in wide-ranging photovoltaic and optoelectronic applications, it is important to note that the tunability of the bandgap of these ultra-small Si structures implies that optical absorption, and hence the optoelectronic performance, of SNS are dependent on the physical structure. Therefore, optical absorption by a solar cell will be dictated by the physical structure of the SNS, which is not fully understood. In this study, we use Time Dependent Density Functional Theory (TDDFT) to investigate the optical properties of SNS, from quantum dots to nanowires. The effect of doping with P, B, and Zr on the optical response of SNS is also investigated, and is seen to show remarkable behavior, and potential to tailor the response. Tailoring of the absorption spectra is very important in the field of plasmonics and photovoltaic applications. At the same time, TDDFT calculations provide a natural framework for the calculation of the exciton binding energy, and its inclusion in the calculation of optical absorption. It is worth mentioning that all the reported exciton binding energies either use empirical formulas or time independent DFT calculations. The infrared (IR) spectra are also calculated and correlated to the experimental results. Furthermore, we investigate how the exciton binding energies, oscillator strength, and molar absorptivity vary with SNS length – from quantum dots to nanowires – and consequently their possible relations to the other quantum confinement effects. Finally, the effects of doping, co-doping, and distance between dopant atoms with P, B, and Zr on both the band gap as well as absorption spectra parameter have been investigated to tailor the absorption spectra.

2. Computational details

TDDFT calculations were performed on [1 1 0] oriented SNS with lengths varying from 1 to 24 *units*. Each *unit* is composed of 24 Si atoms and 16 H atoms, which is the unit cell of a [1 1 0] silicon nanowire (Fig. 1a and b). The two ends of a SNS are terminated by an additional 10 H atoms as can be seen in Fig. 1c. SNS with a crystalline orientation of [1 1 0] show outstanding mechanical and electronic properties (Ma et al., 2003; Adachi et al., 2013; Buin et al., 2008).

All the calculations are performed using Gaussian 09 (Frisch et al., 2009) using B3LYP (Becke, 1993; Lee et al., 1988; Vosko et al., 1980) and the 3-21G (Dobbs and Hehre, 1987) basis set. The hybrid DFT method, B3LYP contains Becke Three Parameter Hybrid Functionals (Becke, 1993) that uses the non-local correlation provided by the LYP expression, (Lee et al., 1988) and local correlation by VWN functional III (Vosko et al., 1980). The geometry optimization process involves using analytical gradients of energy until a stationary point on the potential surface is achieved. During geometry optimization, neither symmetry restriction, nor any other special restrictions to H or Si atoms were implemented. Frequency calculations were performed on the optimized geometry to ensure that it is a local minima on the potential energy surface.

The 3-21G basis set was previously implemented by Sorokin et al. (2008) on a very similar system. The calculated band gaps of the structures with periodic boundary condition (PBC) (shown in Fig. 1a and b) and the longest non-PBC SNS (24 units) in this study are 3.205 eV and 3.229 eV, respectively, which is comparable to 3.5 eV obtained experimentally (Ma et al., 2003). We tested the use of a larger basis set such as 6-31G and find that the band gap for PBC changes to 3.170 eV, which is only about a 1% difference compared to 3-21G basis set. However it

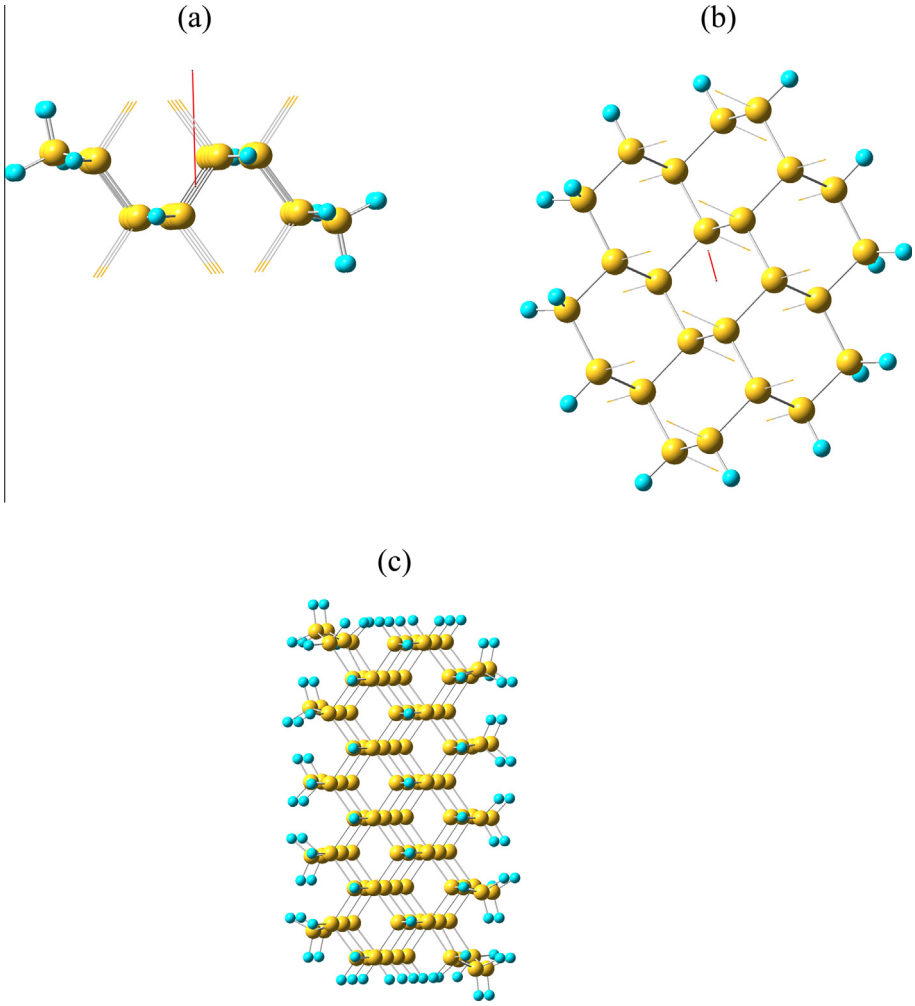


Fig. 1. The (a) side- and (b) top- view of periodic unit cell of a [1 1 0] oriented nanowire. (c) Shows a SNS with 5 units of (a), which is terminated by 10 hydrogen atoms at the top and bottom ends. Orange and cyan spheres represent the Si and H atoms respectively. The red line shows the translational vector to create a PBC. (For interpretation of the references to color in this figure legend, the reader is referred to the web version of this article.)

was seen to consume approximately 230% more computational time, which make the TDDFT calculation with larger basis set computationally infeasible for the larger structures. Another way to show the adequacy of the selection of 3-21G as a basis set is the relatively small change in the length of the unit cell from 3.94 Å using 3-21G, to 4.01 Å using 6-31G using PBC unit cell. On the other hand, for zirconium (Zr) we utilize LANL2DZ as a basis set, which combines Los Alamos effective core potential (ECP) as well as to double zeta (DZ) (Hay and Wadt, 1985a,b; Wadt and Hay, 1985).

The electronic absorption spectra were obtained by Gauss view 5.0.9 (Dennington et al., 2009) using UV–VIS peak half-width at half height of 0.16 eV and 50 excited states. The calculated percentage of the contribution of the molecular orbital transition in each excited state (shown in Table 1) were obtained by taking the square of the coefficient for both excitation and deexcitation terms, which in total is equal to 1 (100%). This is due to the normalization condition in TDDFT calculation:

$$\langle X + Y | X - Y \rangle = 1,$$

where X are the "excitations" and Y the "de-excitations". The TD expansion differs from that of the other CI methods in that the wavefunction includes determinants for both "excitation" and "de-excitation" terms. The G09 output for TD calculations prints the coefficients of both types of terms, X and Y, separately.

3. Results and discussion

3.1. Ground state calculations

The energy of the highest occupied molecular orbital (HOMO) and lowest unoccupied molecular orbital (LUMO) as a function of the number of unit cells in the SNS are summarized in Table 1. Band gap is taken as the difference between energies of LUMO and HOMO, which decreases from 5.4 eV for 1 unit to about 3.2 eV for 24 units (which was the maximum based on computa-

Table 1
HOMO, LUMO, and bandgap energies (ΔE) obtained by DFT, and excitation energies (E), oscillator strengths for the first excited state (f) and strength of optically active states (*Coefficient*) obtained by TDDFT.

# Units	DFT			TDDFT			
	E_{HOMO} (eV)	E_{LUMO} (eV)	ΔE (eV)	State no.	E (eV)	f	MO
1	−6.655	−1.175	5.480	1	4.8149	0.0000	H → L (95%)
				2	5.0206	0.1105	H → L+1 (93%)
2	−6.382	−1.564	4.818	1	4.2218	0.0000	H → L (96%)
				3	4.3225	0.0003	H → L+2 (98%)
				5	4.3511	0.0088	H → L+4 (98%)
4	−6.192	−2.030	4.163	1	3.6614	0.0003	H → L (97%)
6	−6.040	−2.330	3.711	1	3.2559	0.0001	H → L (97%)
8	−5.982	−2.492	3.490	1	3.0708	0.0001	H → L (96%)
10	−5.960	−2.586	3.373	1	2.9820	0.0002	H → L (95%)
12	−5.949	−2.638	3.311	1	2.9428	0.0006	H → L (92%)
							H−2 → L+1 (93%)
14	−5.942	−2.665	3.277	1	2.9199	0.0014	H → L (89%)
							H−1 → L+1 (5%)
16	−5.935	−2.677	3.257	1	2.9134	0.0028	H → L (84%)
							H−1 → L+1 (7%)
							H−4 → L (5%)
18	−5.927	−2.682	3.245	1	2.9173	0.0051	H → L (78%)
							H−1 → L+1 (10%)
							H−4 → L (6%)
20	−5.921	−2.684	3.238	1	2.9153	0.0078	H → L (72%)
							H−1 → L+1 (12%)
							H−3 → L (8%)
							H−3 → L+2 (2%)
24	−5.910	−2.681	3.229	1	2.9124	0.0134	H → L (64%)
							H−1 → L+1 (16%)
							H−3 → L (9%)
							H−3 → L+2 (4%)
							H−5 → L+1 (2%)
∞	−5.851	−2.645	3.205	N/A			

tion limitation). From Table 1, the band gap for SNW composed of 20 units is seen to be almost 60% lower than that for the 1 unit Si quantum dot.

The total energies, E_T, of SNS are also summarized in supplementary material Table S1. In general, absolute value of E_T is both basis set and method dependent. On the other hand, the difference between E_T of two consecutive SNS is expected to be comparable to the total energy of SNS at PBC, which is −6921.617224 a.u. It was found that the total energy difference decreases (from −6921.63028 a.u. (for 2 units minus 1 unit) to −6921.61716 a.u. (for 20 units minus 19 unit)) as length of SNW increases, which can be explained from the slight decrease in the binding energy between SNS repeating units with length. In case of long SNS, particularly when the number of repeating units >17, the binding energies become almost constant, and the total energy difference becomes almost equal to total energy of SNS at PBC.

The theoretical IR spectra of SNS with five units is shown in Fig. 2. The weak intensity bands at frequencies smaller than 500 cm^{-1} are related to Si–Si skeleton vibrations and stretching vibrations. They are characterized by a very weak IR molar absorptivity. This agrees with experimentally measured Si–Si stretching mode of 516 cm^{-1} (Park et al., 2009). The group of bands in the range 550–750 cm^{-1} and 900–950 cm^{-1} are related to Si–H bending vibration. The bands in the range from about 2150 cm^{-1} to 2250 cm^{-1} are related to Si–H stretching vibration (Milekhin et al., 1999).

The above values agree with the experimentally determined FT-IR values for amorphous silicon thin film that showed that Si–H has three groups of bands (Srinivasan and Parsons, 1995). The first band is observed around 635 cm^{-1}, which is due to Si–H bending (Srinivasan and Parsons, 1995; Xu et al., 2006). The bands at 845 and 890 cm^{-1} are due to Si–H_2 vibrations (Srinivasan and Parsons, 1995; Rabha et al., 2005). The band for Si–H stretching mode is reported around 2100 cm^{-1} in different poly-crystalline SNS and Si thin films (Srinivasan and Parsons, 1995; Xu et al., 2006; Rabha et al., 2005). It is worth mentioning that all bands above 550 cm^{-1} do not involve a significant movement of Si atoms. It is possible that the bands around 900 cm^{-1} may have been observed by Park et al. (2009) as a very small band at 957 cm^{-1} and was perhaps miss-assigned as the stretching mode of amorphous Si–Si. In their study, prepared SNS are covered mainly with C atoms rather than H or SiO_2, which may have contributed to the observed small intensity. A similar

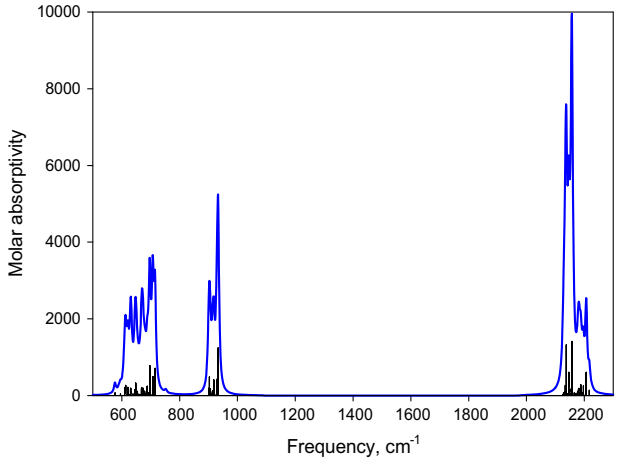


Fig. 2. The theoretical IR spectra for five units of SNS respectively.

IR spectra composed of three group of bands were observed for other SNS (see supplementary material Fig. S1).

3.2. Electronic absorption spectra

The first singlet electronic absorption transition of SNS as a function of length is calculated using TDDFT method and summarized in Table 1. For a very short SNS, the transition from HOMO to LUMO gives rise to a dark state. On the other hand, for SNS with slightly longer lengths (with number of units greater than 11 units), the HOMO–LUMO contribution starts to be optically active in the first singlet excited state S_1. As a general trend, the absorption band shifts to smaller energy values with length, and reaches a limiting value at approximately 425 nm (2.9 eV). It is worth mentioning that the main contribution to S_1 originates from HOMO to LUMO excitation for the lengths considered. Furthermore, as the length increases, $H-1 \rightarrow L+1$ and $H-3 \rightarrow L$ contributions cannot be neglected but remain weaker than the $H \rightarrow L$ contribution. As an example a 5% contribution from HOMO−1 to LUMO+1 starts to be detected at more than 14 units, and increases to 12% at 20 units, where a newer contribution of 8% from the HOMO−3 to LUMO appears (see Table 1). This is because as the length increases, the optical bands move to longer wavelengths and accumulate in S_1. The molecular orbital plots of HOMO and LUMO are shown in (Fig. S2 supplementary material). The plots show that LUMO orbital changes from being localized over length to the diameter with the increase of repeating units.

The exciton binding energy is defined here as the *difference* between the HOMO–LUMO energy (ΔE in column 4 of Table 1) and the corresponding excitation energy from TDDDT (column 6 of Table 1). The exciton binding energy was found to decrease from 0.67 eV for 1 unit to about 0.3 eV for the longest SNS. This agrees with previously reported theoretical data of about 0.2 eV for extremely long SiNW (Parkash et al., 2011). Fig. 3 shows the increase of the oscillator strength of S_1 and S_4 as a function of the number of repeating units. The S_2 and S_3 are dark states regardless of the number of repeating units. The S_1 is an almost dark state in the SNS with length <11 units, and its oscillator strength grows dramatically with length after that. The increase in oscillator strength follows first a quadratic (solid line) and then a linear trend (dashed line) for medium and long SNS. A similar trend is observed for S_4. The transition dipole moment for the small SNS is localized over the SNS diameter, while transitions for longer SNS are localized over the length. This may be the reason for the change in the dependence of the oscillator strength with length. Explanation of this phenomenon can be obtained by using the simplified PIB model to calculate the transition dipole moment as a function of the box length, which results in the transition dipole moment being proportional to the length (supplementary material).

Fig. 4 shows the effect of length on the electronic absorption spectra of SNS. The spectra of SNS with 4, 8, and 10 units show the increase in the oscillator strength for all states with increase in length. It is worth mentioning that the spectra of SNS with 15, 20, and 24 units do not have enough number of excited states to show all the bands observed for smaller number of units. However, they still clearly show the growth of the oscillator strength of S_1 with length, as explained before in Fig. 3. The quantum confinement effect results in the movement of all the band locations to higher wavelength with length increase. This process eventually leads to accumulation of more contributions in S_1 as shown in Table 1. In summary, the spectra show two simultaneous overlapping phenomena with the length increase. The first is the increase of the oscillator strength for all states. The second is band movement to longer wavelength till it reaches a limiting frequency.

3.3. Effect of doping

Doping a SNS is seen to produce a very dramatic effect on its optical absorption, Here, we study the effect of dop-

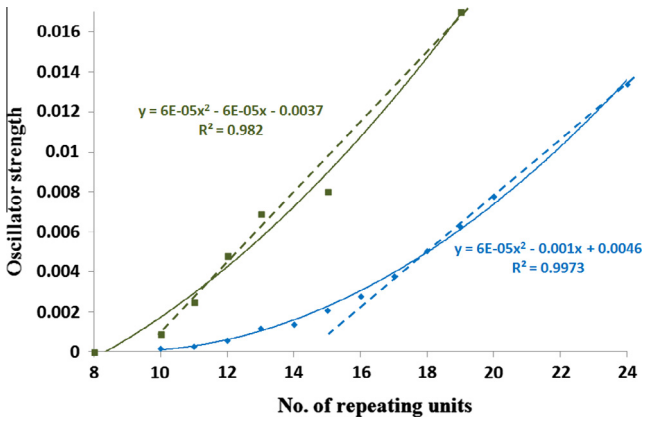


Fig. 3. The oscillator strength of S_1 (blue lines) an S_4 (green lines) as a function of number of repeating units. (For interpretation of the references to color in this figure legend, the reader is referred to the web version of this article.)

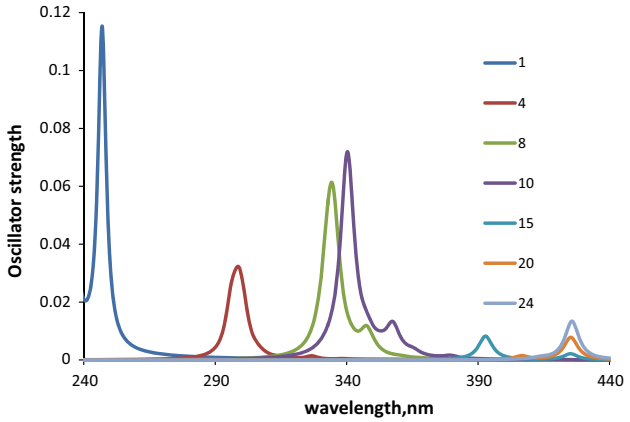


Fig. 4. Theoretically calculated electronic absorption spectrum of SNS with different number of repeating units.

ing SNS with 2, 5, and 20 unit cells with different combinations of P, B, and Zr atoms. Doping was achieved by replacing one Si atom at the center of the SNS by a dopant atom, followed by full geometry optimization. The energetic parameters for the optimized SNS are summarized in Table S2 in supplementary material. On adding one P or B atom the total number of electrons becomes odd, which results in open shell calculations with two different spins, α and β, for both HOMO and LUMO energy levels. The direct band gap ΔE is taken as the minimum energy difference between the LUMO and the HOMO, having the same spin. It is worth mentioning that, if band gap is calculated using different spins it will produce an optically spin forbidden transition (dark excited state). As a general trend, all the doped SNS have a smaller band gap and higher dipole moment than pure SNS. Doping with either P or B atom alone dramatically decreases the band gap by approximately 27% or 18%, respectively. On the other hand, doping with Zr decreases the band gap approximately by 70% relative to the intrinsic SNS. A double doping, with one P and one B atom together, slightly decreases the band gap to about 90% relative to intrinsic SNS. The band gap is seen to decrease with dopants in the following order: B < P < BZr < PZr < Zr < BP < pure SNS, regardless of SNS length. Careful inspection of the energies of HOMO and LUMO for B and P shows that a P atom lowers the band gap by introducing higher HOMO of α spin, while in case of a B atom the lowering is due to an introduction of lower LUMO with β spin (see supplementary material Fig. S3). Doping with Zr adds a lower LUMO without changing the orbital spin. On the other hand, codoped B and P SNS shows almost a similar band gap to pure silicon SNS. It is worth mentioning that as the distance between the B and P atoms increases, the band gap decreases. This may shift the band gap of codoped B–P SNS to be slightly lower than Zr doped SNS, but even for the case when the distance between the atoms is relatively large, the band gap remains higher than in case of PZr doped SNS. The codoping with stoichiometric ratio of B and P atoms results in full overlap between the HOMO from P atom with the LUMO of B atom, resulting in larger band gap compared to doping only with either B or P.

The normalized electronic absorption spectrum calculated using TDDFT for pure as well as doped SNSs with 2 units are shown in Fig. 5. The normalized spectra is the spectra from the G09 calculations divided by the number of repeating units. The pure SNS shows only one peak at approximately 260 nm. The addition of just one Zr atom not only shifts this band to 330 nm, but also produces a new band at about 410 nm relative to undoped SNS, approximately in the visible spectrum. Doping with B results in a similar effect, but the new band shows an even more drastic shift to 600 nm.

In case of P, the spectra is very distorted with 4 major peaks at 340 nm, 390 nm, 490 nm, and 560 nm. More importantly, the spectra becomes significantly broad, and shows that the SNS converts from an almost non-absorber to a very significant absorber of visible light.

The spectra of ZrP and ZrB are quite similar to each other since they are composed of 2 bands. In case of ZrP the two bands are approximately at 400 nm and 500 nm, while in case of ZrB they shift to higher wavelengths of 440 nm and 530 nm. A comparison of these numbers leads to the conclusion that the first bands of ZrP and ZrB may originate from Zr itself. The spectra of ZrB can be considered as additive spectra, where band originating from Zr at 410 nm mixes with band of B at 600 nm, to form a new band at 530 nm. On the other hand, the spectra of ZrP is not additive. The presence of P and B atoms together diminish their individual effects to a great extent, resulting in a spectrum that is much similar to undoped SNS, but with two noticeable differences. The first is a small shift of spectra to higher wavelength, while the second is a small weak tail at 340 nm.

The effect of the distance between B and P on the absorption spectra was also studied, where 'PB', 'PBd' and 'PBd2' shown in Fig. 5 refer to different optimized separation distances between P and B atoms of (2.06 Å, 4.45 Å, 8.73 Å) and (2.10 Å, 4.47 Å, 14.11 Å) for 2 and 5

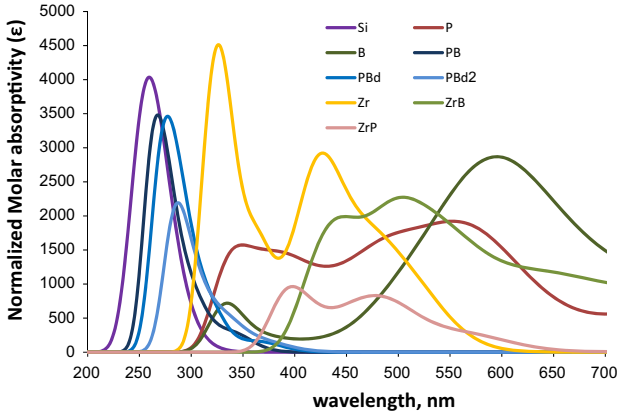


Fig. 5. The normalized electronic absorption spectra of SNS with 2 repeating units having different dopant atoms.

units, respectively. Our calculations show that the bonded co-doped B and P SNS (i.e. the one having the smallest possible separation between B and P) is more stable than the case where B and P are separated by large distances, by 9.5 and 12.2 kcal/mol for 2 and 5 units, respectively (see supplementary material Tables S3 and S4). The energy required to separate the B and P atoms increase with separation distance, which explains why the separation energy of the structure with 5-units is more than the case with 2 units. This data agrees with the recent study done by Fukata et al. (2013) using molecular dynamics, which reported that doping with both B and P leads eventually to the formation of a B–P chemical bond that stabilizes the doped atoms in the Si side, inhibiting its diffusion to the SiO_2 layer. As a consequence of the band gap decrease with increase of the distance between B and P, the main absorption band shifts to higher wavelength. For bonded co-doped B–P the spectra is very similar to undoped SNS.

On integrating the molar absorption coefficient in Fig. 5 in the visible wavelengths (400–700 nm), we obtain total absorbance in visible region. The total absorbance for different dopants in decreasing order is: ZrB > P > B > Zr ≫ ZrP ≫ intrinsic SNS. It is worth mentioning that a very similar trend is observed in the case of 5 and 20 units of SNS (see supplementary material Fig. S4). The normalized molar absorptivity in Figs. 5 and S4 revealed two facts with increasing the number of repeating units, the expected bathochromic (red) shift due to quantum confinement effect and surprisingly, hypochromic shift. This may indicate the better efficiency of relatively smaller quantum dots over larger ones as light absorbers, which is experimentally observed by Sheng et al. (2014), Borgström et al. (2005), Greenman et al. (2013) and Sorokin et al. (2008).

4. Conclusions

In conclusion, the effects of the physical structure and doping on the potential to tailor the optical response of silicon nanostructures (SNSs) have been investigated. The length of a SNS plays an important role in tailoring the band gaps. The band gap is seen to decrease with SNS length for the same diameter, until the length becomes greater than 8 times the diameter (where the number of repeating units is larger than 18), at which point the band gap becomes almost independent of length. TDDFT calculations show that the optical absorption band moves to higher wavelength with an increase in SNS length, and eventually become almost constant for long SNS. Furthermore, the appearance of more configurations in longer SNS than the shorter ones leads to overlapped states in S_1. Photon with polarization along the length of SNS is most effective in causing HOMO to LUMO excitation, and the oscillator strength and molar absorptivity increase quadratically for medium SNS (with units between 10 and 16 units), and then linearly for SNS larger than $\geqslant$18 units. The observed absorption spectra obtained by TDDFT appear at slightly smaller wavelength than HOMO–LUMO energy gap difference, and this difference can be related to exciton binding energy. The exciton binding energy dramatically decreases with the length. Results suggest a higher optical absorption in longer SNS than in shorter ones. The theoretical IR spectra showed that Si–Si bond vibration appears at lower wave number than Si–H bond vibration. This is due to the greater difference in the reduced mass of Si–Si, which is 14 times more than that of Si–H.

A significant optical effect is found in the case of dopedSNSs. Here the absorption is found to move significantly from the high frequency spectrum for intrinsic SNS, to the visible spectrum for SNS doped with either P or B. Furthermore, the absorption spectra and total absorption can potentially be further tailored through single and double doping of the SNSs. For example, the ratios of total absorption of doped ZrB over doped ZrP 2 and 5 units cell SNS are 3.6 and 4.4, respectively. On the other hand, the same SNS are completely transparent in visible region for both pure and PB doped SNS. This implies that a controlled doping of small SNS may make them highly efficient solar cell or other optoelectronic materials, adapted for particular applications.

Acknowledgements

This paper was made possible by a NPRP Grant # 5-968-2-403 from the Qatar National Research Fund (a member of Qatar Foundation). The statements made herein are solely the responsibility of the authors. The calculations were performed on a 32 Core, 128 GB RAM machine with dual Xeon E5-2680 CPUs. The authors acknowledge the generous research computing support through the use of the supercomputer Stampede from the Texas Advanced Computing Center (TACC) at The University of Texas at Austin through Texas A&M University – Kingsville.

Appendix A. Supplementary material

Supplementary data associated with this article can be found, in the online version, at http://dx.doi.org/10.1016/j.solener.2015.11.030.

References

Adachi, M.M., Anantram, M.P., Karim, K.S., 2010. Optical properties of crystalline–amorphous core–shell silicon nanowires. Nano Lett. 10, 4093–4098.

Adachi, M.M., Anantram, M.P., Karim, K.S., 2013. Core–shell silicon nanowire solar cells. Sci. Rep. 3 (1546), 1–6.

Becke, A.D., 1993. Density-functional thermochemistry. III. The role of exact exchange. J. Chem. Phys. 98, 5648–5652.

Borgström, M.T., Zwiller, V., Müller, E., Imamoglu, A., 2005. Optically bright quantum dots in single nanowires. Nano Lett. 5 (7), 1439–1443.

Buin, A.K., Verma, A., Svizhenko, A., Anantram, M.P., 2008. Significant enhancement of hole mobility in [1 1 0] silicon nanowires compared to electrons and bulk silicon. Nano Lett. 8, 760–765.

Conibeer, G., Green, M., Cho, E.-C., König, D., Cho, Y.-H., Fangsuwannarak, T., Scardera, G., Pink, E., Huang, Y., Puzzer, T., Huang, S., Song, D., Flynn, C., Park, S., Hao, X., Mansfield, D., 2008. Silicon quantum dot nanostructures for tandem photovoltaic cells. Thin Solid Films 516, 6748–6756.

Cui, Y., Duan, X., Hu, J., Lieber, C.M., 2000. Doping and electrical transport in silicon nanowires. J. Phys. Chem. B 104 (22), 5213–5216.

Cui, Y., Zhong, Z., Wang, D., Wang, W.U., Lieber, C.M., 2003. High performance silicon nanowire field effect transistors. Nano Lett. 3, 149–152.

Cullis, A.G., Canham, L.T., 1991. Visible light emission due to quantum size effects in highly porous crystalline silicon. Nature 335, 335–338.

Dennington, R., Keith, T., Millam, J., 2009. GaussView, Version 5. Semichem Inc., Shawnee Mission, KS.

Dobbs, K.D., Hehre, W.J., 1987. Molecular-orbital theory of the properties of inorganic and organometallic compounds. 6. Extended basis-sets for 2nd-row transition-metals. J. Comput. Chem. 8, 880–893.

Dybiec, M., Ostapenko, S., Torchynska, T.V., Losada, E.V., 2004. Scanning photoluminescence spectroscopy in InAs/InGaAs quantum-dot structures. Appl. Phys. Lett. 84, 5165–5167.

Frisch, M.J., Trucks, G.W., Schlegel, H.B., Scuseria, G.E., Robb, M.A., Cheeseman, J.R., Scalmani, G., Barone, V., Mennucci, B., Petersson, G.A., Nakatsuji, H., Caricato, M., Li, X., Hratchian, H.P., Izmaylov, A.F., Bloino, J., Zheng, G., Sonnenberg, J.L., Hada, M., Ehara, M., Toyota, K., Fukuda, R., Hasegawa, J., Ishida, M., Nakajima, T., Honda, Y., Kitao, O., Nakai, H., Vreven, T., Montgomery Jr., J.A., Peralta, J.E., Ogliaro, F., Bearpark, M., Heyd, J.J., Brothers, E., Kudin, K.N., Staroverov, V.N., Kobayashi, R., Normand, J., Raghavachari, K., Rendell, A., Burant, J.C., Iyengar, S.S., Tomasi, J., Cossi, M., Rega, N., Millam, J.M., Klene, M., Knox, J.E., Cross, J. B., Bakken, V., Adamo, C., Jaramillo, J., Gomperts, R., Stratmann, R. E., Yazyev, O., Austin, A.J., Cammi, R., Pomelli, C., Ochterski, J.W., Martin, R.L., Morokuma, K., Zakrzewski, V.G., Voth, G.A., Salvador, P., Dannenberg, J.J., Dapprich, S., Daniels, A.D., Farkas, Ö., Foresman, J.B., Ortiz, J.V., Cioslowski, J., Fox, D.J., 2000. Gaussian 09, Revision D.01. Gaussian Inc., Wallingford, CT.

Fukata, N., Kaminaga, J., Takiguchi, R., Rurali, R., Dutta, M., Murakami, K., 2013. Interaction of boron and phosphorus impurities in silicon nanowires during low-temperature ozone oxidation. J. Phys. Chem. C 117, 20300–20307.

Garcia-Lastra, J.M., Thygesen, K.S., 2011. Renormalization of optical excitations in molecules near a metal surface. Phys. Rev. Lett. 106, 187402, Erratum 2011. Phys. Rev. Lett. 107, 179901.

Greenman, L., Whitley, H.D., Whaley, K.B., 2013. Large-scale atomistic density functional theory calculations of phosphorus-doped silicon quantum bits. Phys. Rev. B 88, 165102.

Hao, X.J., Cho, E.-C., Flynn, C., Shen, Y.S., Park, S.C., Conibeer, G., Green, M.A., 2009a. Synthesis and characterization of boron-doped Si quantum dots for all-Si quantum dot tandem solar cells. Sol. Energy Mater. Sol. Cells 93, 273–279.

Hao, X.J., Cho, E.-C., Scardera, G., Shen, Y.S., Bellet-Amalric, E., Bellet, D., Conibeer, G., Green, M.A., 2009b. Phosphorus-doped silicon quantum dots for all-silicon quantum dot tandem solar cells. Sol. Energy Mater. Sol. Cells 93, 1524–1530.

Hay, P.J., Wadt, W.R., 1985a. Ab initio effective core potentials for molecular calculations – potentials for the transition-metal atoms Sc to Hg. J. Chem. Phys. 82, 270–283.

Hay, P.J., Wadt, W.R., 1985b. Ab initio effective core potentials for molecular calculations – potentials for K to Au including the outermost core orbitals. J. Chem. Phys. 82, 299–310.

Kanemitsu, Y., Okamoto, S., 1997. Resonantly excited photoluminescence from porous silicon: effects of surface oxidation on resonant luminescence spectra. Phys. Rev. B 56, R1696(R).

Kim, J.H., Jeon, K.A., Choi, J.B., Lee, S.Y., 2003. Laser wavelength and partial pressure effects on the formation of nanocrystalline Si. Mater. Sci. Eng. B 101, 146–149.

Kocevski, V., Eriksson, O., Rusz, J., 2013. Transition between direct and indirect band gap in silicon nanocrystals. Phys. Rev. B 87, 245401.

Kupchak, I.M., Korbutyak, D.V., Kryuchenko, Y.V., Sachenko, A.V., Sokolovskiĭ, I.O., Sreseli, O.M., 2006. Exciton characteristics and exciton luminescence of silicon quantum dot structures. Semiconductors 40 (1), 94–103.

Lee, C., Yang, W., Parr, R.G., 1988. Development of the Colle-Salvetti correlation-energy formula into a functional of the electron density. Phys. Rev. B 37, 785–789.

Lehmann, V., Gosele, U., 1991. Porous silicon formation: a quantum wire effect. Appl. Phys. Lett. 58, 856–858.

Lu, Z.H., Lockwood, D.J., Baribeau, J.-M., 1995. Quantum confinement and light emission in SiO_2/Si superlattices. Nature 378, 258–260.

Ma, D.D.D., Lee, C.S., Au, F.C.K., Tong, S.Y., Lee, S.T., 2003. Small-diameter silicon nanowire surfaces. Science 299, 1874–1877.

Milekhin, A., Friedrich, M., Hiller, K., Wiemer, M., Gessner, T., Zahn, D. R.T., 1999. Infrared study of Si surfaces and bonded Si wafers. Semicond. Sci. Technol. 14 (1), 70–73.

Park, G.-S., Kwon, H., Lee, E.K., Kim, S.K., Lee, J.H., Li, X.S., Chung, J.G., Heo, S., Song, I.Y., Lee, J.H., Choi, B.L., Kim, J.M., 2010. Fabrication of surface plasmon-coupled Si nanodots in Au-embedded silicon oxide nanowires. Adv. Mater. 22, 2421–2425.

Park, M.-H., Kim, M.G., Joo, J., Kim, K., Kim, J., Ahn, S., Cui, Y., Cho, J., 2009. Silicon nanotube battery anodes. Nano Lett. 9 (11), 3844–3847.

Parkash, V., Kulkarni, A.K., 2011. Optical absorption characteristics of silicon nanowires for photovoltaic applications. IEEE Trans. Nanotechnol. 10 (6), 1293–1297.

Prokes, S.M., 1993. Light emission in thermally oxidized porous silicon: evidence for oxide-related luminescence. Appl. Phys. Lett. 62, 3244–3246.

Rabha, M.B., Saadoun, M., Boujmil, M.F., Bessaïs, B., Ezzaouia, H., Bennaceur, R., 2005. Application of the chemical vapor-etching in polycrystalline silicon solar cells. Appl. Surf. Sci. 252, 488–493.

Rand, B.P., Genoe, J., Heremans, P., Poortmans, J., 2007. Solar cells utilizing small molecular weight organic semiconductors. Prog. Photovolt.: Res. Appl. 15, 659–676.

Reining, L., Olevano, V., Rubio, A., Onida, G., 2002. Excitonic effects in solids described by time-dependent density-functional theory. Phys. Rev. Lett. 88, 066404.

Schuppler, S., Friedman, S.L., Marcus, M.A., Adler, D.L., Xie, Y.-H., Ross, F.M., Chabat, Y.J., Harris, T.D., Brus, L.E., Brown, W.L., Chaban, E.E., Szajowski, P.F., Christman, S.B., Citrin, P.H., 1995. Size, shape, and composition of luminescent species in oxidized Si nanocrystals and H-passivated porous Si. Phys. Rev. B 52, 4910–4925.

Shcherbyna, L., Torchynska, T., 2013. Si quantum dot structures and their applications. Physica E 51, 65–70.

Sheng, W., Sun, B., Shi, T., Tan, X., Peng, Z., Liao, G., 2014. Quantum dot-sensitized hierarchical micro/nanowire architecture for photoelectrochemical water splitting. ACS Nano 8 (7), 7163–7169.

Sivakov, V., Andrä, G., Gawlik, A., Berger, A., Plentz, J., Falk, F., Christiansen, S.H., 2009. Silicon nanowire-based solar cells on glass: synthesis, optical properties, and cell parameters. Nano Lett. 9, 1549–1554.

Sorokin, P.B., Avramov, P.V., Chernozatonskii, L.A., Fedorov, D.G., Ovchinnikov, S.G., 2008. Atypical quantum confinement effect in silicon nanowires. J. Phys. Chem. A 112, 9955–9964.

Srinivasan, E., Parsons, G.N., 1995. Active matrix liquid crystal displays, 25–26 Sept. AMLCDs '95, Second International Workshop.

Torchinskaya, T.V., Aguilar-Hernandez, J., Hernández, L.S., Polupan, G., Goldstein, Y., Many, A., Jedrzejewski, J., Kolobov, A., 2003. Mechanism of photoluminescence of silicon oxide films enriched by Si or Ge. Microelectron. Eng. 66, 83–90.

Torchynska, T.V., Sheinkman, M.K., Korsunskaya, N.E., Khomenkovan, L.Y., Bulakh, B.M., Dzhumaev, B.R., Many, A., Goldstein, Y., Savir, E., 1999. OH-related emitting centers in interface layer of porous silicon. Physica B 273–274, 955–958.

Torchynska, T.V., Hernandez, A.V., Dybiec, M., Emirov, Y., Tarasov, I., Ostapenko, S., Matsumoto, Y., 2005. Optical characterization of

crystalline silicon embedded in a-Si matrix. Phys. Status Solidi C 2 (6), 1832–1836.

Torchynska, T.V., Cano, A.D., Dybic, M., Ostapenko, S., Mynbaeva, M., 2006. Stimulation of excitonic and defect-related luminescence in porous SiC. Physica B 376–377, 367–369.

Trani, F., Cantele, G., Ninno, D., Iadonisi, G., 2005. Tight-binding calculation of the optical absorption cross section of spherical and ellipsoidal silicon nanocrystals. Phys. Rev. B 72, 075423.

Tsakalakos, L., Balch, J., Fronheiser, J., Shih, M.-Y., LeBoeuf, S.F., Pietrzykowski, M., Codella, P.J., Korevaar, B.A., Sulima, O., Rand, J., Davuluru, A., Rapol, U., 2007. Strong broadband optical absorption in silicon nanowire films. J. Nanophotonics 1 (1), 1–10.

Vosko, S.H., Wilk, L., Nusair, M., 1980. Accurate spin-dependent electron liquid correlation energies for local spin density calculations: a critical analysis. Can. J. Phys. 58, 1200–1211.

Wadt, W.R., Hay, P.J., 1985. Ab initio effective core potentials for molecular calculations – potentials for main group elements Na to Bi. J. Chem. Phys. 82, 284–298.

Wang, D., Dai, H., 2006. Germanium nanowires: from synthesis surface chemistry, and assembly to devices. Appl. Phys. A 85, 217–225.

Weissker, H.-Ch., Furthmüller, J., Bechstedt, F., 2002. Optical properties of Ge and Si nanocrystallites from ab initio calculations. II. Hydrogenated nanocrystallites. Phys. Rev. B 65, 155328.

Wong, B.M., 2009. Optoelectronic properties of carbon nanorings: excitonic effects from time-dependent density functional theory. J. Phys. Chem. C 113, 21921–21927.

Xie, P., Hu, Y., Fang, Y., Huang, J., Lieber, C.M., 2009. Diameter-dependent dopant location in silicon and germanium nanowires. PNAS 106 (36), 15254–15258.

Xu, J., Mei, J., Rui, Y., Chen, D., Cen, Z., Li, W., Ma, Z., Xu, L., Huang, X., Chen, K., 2006. UV and blue light emission from SiC nanoclusters in annealed amorphous SiC alloys. J. Non-Cryst. Solids 352, 1398–1401.

Zheng, G., Lu, W., Jin, S., Lieber, C.M., 2004. Synthesis and fabrication of high-performance n-type silicon nanowire transistors. Adv. Mater. 16, 1890–1893.